

# X-ray/UV CAMPAIGN ON THE MRK 279 AGN OUTFLOW: CONSTRAINING INHOMOGENEOUS ABSORBER MODELS

Nahum Arav<sup>1</sup>, Jelle Kaastra<sup>2</sup>, Gerard A. Kriss<sup>3</sup>, Kirk T. Korista<sup>4</sup>, Jack Gabel<sup>1</sup>, Daniel Proga<sup>5</sup>

## ABSTRACT

We investigate the applicability of inhomogeneous absorber models in the formation of AGN outflow absorption-troughs. The models we explore are limited to monotonic gradients of absorbing column densities in front of a finite emission source. Our main finding is that simple power-law and gaussian distributions are hard pressed to fit the Mrk 279 high-quality UV outflow data. An acceptable fit for the O VI troughs can only be obtained by assuming unrealistic optical depth values (upward of 100). The strongest constraints arise from the attempt to fit the Lyman series troughs. In this case it is evident that even allowing for complete freedom of both the power-law exponent and the optical depth as a function of velocity cannot yield an acceptable fit. In contrast, partial covering models do yield good fits for the Lyman series troughs. We conclude that monotonic inhomogeneous absorber models that do not include a sharp edge in the optical depth distribution across the source are not an adequate physical model to explain the trough formation mechanism for the outflow observed in Mrk 279.

## 1. INTRODUCTION

AGN outflows are evident by resonance line absorption troughs, which are blueshifted with respect to the systemic redshift of their emission counterparts. In Seyfert galaxies velocities of several hundred  $\text{km s}^{-1}$  (Crenshaw et al. 1999; Kriss et al. 2000) are typically observed in both UV resonance lines (e.g., C IV  $\lambda\lambda 1548.20, 1550.77$ , N V  $\lambda\lambda 1238.82, 1242.80$ , O VI  $\lambda\lambda 1031.93, 1037.62$  and  $\text{Ly}\alpha$ ), as well as in X-ray resonance lines (Kaastra et al. 2000, 2002; Kaspi et al. 2000, 2002). Similar outflows (often with significantly higher velocities)

---

<sup>1</sup>CASA, University of Colorado, 389 UCB, Boulder, CO 80309-0389, I:arav@colorado.edu

<sup>2</sup>SRON National Institute for Space Research Sorbonnelaan 2, 3584 CA Utrecht, The Netherlands

<sup>3</sup>STScI, Baltimore, MD 21218

<sup>4</sup>Western Michigan Univ., Dept. of Physics, Kalamazoo, MI 49008-5252

<sup>5</sup>JILA, University of Colorado, Boulder, CO 80309

are seen in quasars which are the luminous relatives of Seyfert galaxies (Weymann et al. 1991; Korista, Voit, Morris, & Weymann 1993; Arav et al. 2001a). Reliable measurement of the absorption column densities in the troughs is crucial for determining the ionization equilibrium and abundances of the outflows, and the relationship between the UV and the ionized X-ray absorbers.

In the last few years our group (Arav 1997; Arav et al. 1999a; Arav et al. 1999b; de Kool et al. 2001; Arav et al. 2002, 2003) and others (Barlow 1997, Telfer et al. 1998, Churchill et al. 1999, Ganguly et al. 1999) have shown that in quasar outflows most lines are saturated even when not black. As a consequence the apparent optical depth method, which stipulates that the optical depth  $\tau_{ap} \equiv -\ln(I)$ , where  $I$  is the residual intensity in the trough, is not a good approximation for outflow troughs. In addition using the doublet method (Barlow 1997, Hamann et al 1997) we have also shown that in many cases the shapes of the troughs are almost entirely due to changes in the line of sight covering as a function of velocity, rather than to differences in optical depth (Arav et al. 1999b; de Kool et al. 2001; Arav et al. 2001a). Gabel et al. (2003) show the same effect in the outflow troughs of NGC 3783, as does Scott et al. (2004) for Mrk 279. As a consequence, the column densities inferred from the depths of the troughs are only lower limits.

Most of the analysis cited above relies on comparing two troughs arising from the doublet lines of a given ion (e.g., the C IV, N V and O VI, doublets mentioned above). Based on the oscillator strength of the doublet components, the blue transition must have twice the optical depth as the red transition. When the apparent optical depth method is used on fully resolved, high S/N, non-blended doublet troughs, the ratio of their  $\tau_{ap}$  is rarely 1:2. In most cases, the trough from the red doublet has more than half of the blue  $\tau_{ap}$ , up to equality in many cases. In order to determine the actual optical depth (and hence column density), we use a pure partial covering model. We assume that only a fraction  $C$  of the emission source is covered by the absorber and then solve for a combination of  $C$  and  $\tau$  that will fit the data of both doublet troughs while maintaining the intrinsic 1:2 optical depth ratio (see § 3 for the full formalism, including velocity dependence). Implicit in this model are the assumptions that the absorber covering the  $C$  fraction of the source has the same optical depth across this area, and that the rest of the source is covered by material with  $\tau = 0$  in that transition.

Although widely used, the validity of the pure partial covering model should be questioned on two fronts. First, mathematically we solve for two unknowns ( $C$  and  $\tau$ ) given two residual intensity equations. As long as the ratio of the residual intensities is in the permitted physical range (see § 3), such a procedure will always yield a solution. A principal issue is, how valid is this solution physically? To test the partial covering model we need more lines from the same ions and efforts in that direction will be described in forthcoming papers (Gabel et al. 2004, Arav et al. 2004). The second question has to do with the rigid distribution (essentially a step-function) of absorbing material assumed by the partial

covering model. Here one may ask if an inhomogeneous distribution of absorbing material across the emission source can yield a good alternative to the partial covering model.

The first attempt to study generic inhomogeneous distributions of absorbing material in AGN outflows was done by de Kool, Korista & Arav (2002, hereafter dKKA). A formalism was developed to simulate the effects of an inhomogeneous absorber on the emerging spectrum and several examples of fitting existing data with this model were presented. In this paper we begin by giving a simplified version of the dKKA formalism, and explain the spectrum arising from simple monotonic material distributions (§ 2). Since little constraints can be put on the formation of a single trough, in § 3 we simulate and explain the formation of doublet troughs. In § 4 we use these simulations in an attempt to fit the O VI, NV and Lyman series troughs seen in high-quality observations of Mrk 279. In light of these results, we assess the physical viability of inhomogeneous absorber models in § 5

## 2. MONOTONIC OPTICAL DEPTH DISTRIBUTIONS

In this section we introduce the formalism needed to calculate the attenuation caused by an inhomogeneous absorbing medium. Our starting point is equation (6) from dKKA:

$$F(\lambda) = \int \int S(x, y, \lambda) e^{-\tau(x, y, \lambda)} dx dy, \quad (1)$$

where  $S(x, y, \lambda)$  is the surface brightness distribution of the background source and  $\tau(x, y, \lambda)$  is the line of sight optical depth at wavelength  $\lambda$  in front of a specific  $(x, y)$  location, as defined by dKKA equations (3-5). We find that the formalism that depends on real spatial variables  $(x, y)$  is simpler and more intuitive than working in  $\tau$  space as was originally done in dKKA (their equations 7-10, 13 and 15).

In its most general form, Equation (1) is not practical for modeling spectra. Both  $S(x, y, \lambda)$  and  $\tau(x, y, \lambda)$  each have two functional degrees of freedom for a given  $\lambda$ . We need a simpler and testable model. To this end, we introduce the following simplifying assumptions and comment about their physical validity and plausibility.

1.  $S(x, y, \lambda) = 1$

This is probably the weakest of our simplifications. For an accretion disk, it is probable that  $S(x, y)$  is a strong function of distance from the central source. Moreover, there are at least two main emission sources at the wavelength range of the absorption troughs: Continuum emission and broad emission line flux. These differ from each other greatly by their physical size and the emissivity as a function of wavelength (see Gabel et al. 2004). Nonetheless, it is essential to at least start with  $S(x, y, \lambda) = 1$  models in order to gain insight about absorption-trough formation in inhomogeneous media.

2.  $\tau(x, y, \lambda) = \tau(x, \lambda)$

This simplifying assumption entails little loss of generality. We can think of  $e^{-\tau(x, \lambda)}$  as the integrated attenuated flux along a  $y$  strip at a specific  $(x, \lambda)$ .

3.  $\tau(x, \lambda) = \tau_{\max}(\lambda)x^a$       or       $\tau(x, \lambda) = \tau_{\max}(\lambda)e^{-(x/b)^2}$

Since there are infinite functional possibilities for the  $\tau(x)$  distribution, we limit our discussion to two simple and well-behaved functional forms. Each of these functions depends on two free parameters. We also discuss a two parameter step function, which is the mathematical representation of the pure partial covering model.

### 2.1. Power-Law, Gaussian and Step-function Distributions

Using the above simplifications, we begin by examining simple monotonic distributions of optical depth in front of a one dimensional emission source. By construction, the emission source spans the interval  $0 < x < 1$  and we assume that the surface brightness distribution is constant over this interval and given by  $S(x, y, \lambda) = 1$  (see discussion above). Finally, for simplicity we ignore the  $\lambda$  (or velocity) dependence of both  $S$  and  $\tau$ . We will examine the role of velocity dependence in § 3. To gain better understanding of the absorption behavior of such a medium we define the following parameters:

1.  $\bar{\tau} \equiv \int_0^1 \tau(x)dx$ , the average optical depth in front of the emission source. This is the relevant quantity for computing and comparing column densities ( $N_{\text{ion}}$ ).
2.  $I \equiv \int_0^1 e^{-\tau(x)}dx$ , the residual intensity of the transmitted flux (normalized to 1 in the absence of absorption) that an observer far from the absorber will measure.
3.  $\tau_{ap} \equiv -\ln(I)$ , apparent optical depth, which is the optical depth inferred from  $I$  assuming a uniform absorbing slab that fully covers the emission source. This is the general case for ISM and IGM absorbers.
4.  $T$ , transmission parameter, measures the fraction of the emission source that is covered by  $\tau < 0.5$ . As we show below, for steep  $\tau(x)$  distributions  $I \simeq T$ . Even more accurately,  $\Delta I \simeq \Delta T$  for two similar distributions with different  $\bar{\tau}$ .

In figure 1 we illustrate several monotonic absorbing-material distributions. The inset table displays some of the parameters defined above that are associated with these distributions. For calculating the transmitted residual flux  $I$ , we divided the emission zone into 1000 elements, calculated  $I$  at each one according to the value of  $\tau$  in front of it, summed all the contributions and normalized by the number of elements. To aid the visualization of such distributions we make the assumption that the number density of the

absorbing ion  $n_{\text{ion}}$  is constant. This allows us to create simple geometrical illustrations of the absorbing-matter distribution, where the optical depth axis is proportional to the spatial depth of the absorber. We note that this assumption does not change the calculation of emergent flux, but in general will affect the conversion of optical depth to total column density.

Following dKKA, for the power-law case we assume that  $\tau_{\text{min}} = 0$ , which reduces the number of free parameters to two:  $\tau_{\text{max}}$ , the maximum optical depth in the distribution, and  $a$ , the power-law exponent. Although for power-law distributions dKKA give closed form solutions for equation (1), these are expressed as the product of gamma functions and incomplete gamma functions (see their eq. 13), which are not particularly illuminating. We therefore rely solely on numerical results and attempt to clarify their origin and significance. To ease comparison with the power law case, the actual gaussian distribution plotted is  $\tau(x) = \tau_{\text{max}} e^{-[(x-1)/b]^2}$ , with no loss of generality.

The amount of material in each distribution is given by  $\bar{\tau}$ , and the ratio  $\bar{\tau}/\tau_{ap}$  can be interpreted as the amount of material “hidden” in the inhomogeneous absorber compared to what we naively deduce by using  $\tau_{ap}$ . As we show with real data (see § 4), this ratio can become very large when attempting to fit doublet troughs with power-laws and gaussian distributions. For all plotted distributions we note the similarity in value between  $I$  and  $T$ . The plotted step function shows the inhomogeneous absorber representation of a pure partial covering.

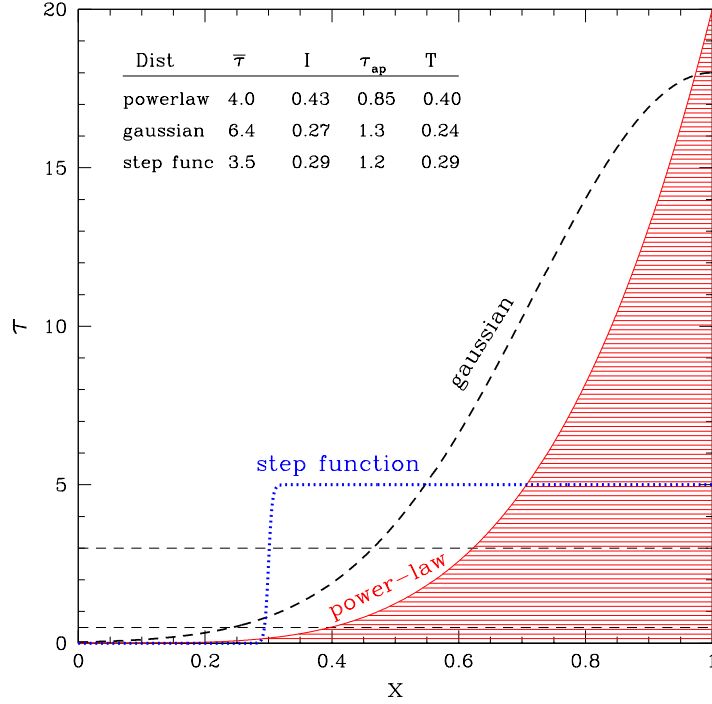


Fig. 1.— Several monotonic distributions of absorbing material in front of an emission source. The constant emission source coincides with the  $x$  axis, and the observer is far above the plot. For the power-law case we shaded the region of absorbing material, and for all distributions the absorbing material is below the curve. For each distribution the optical depth in front of an  $x$  location is given by:

Power-law:  $\tau(x) = \tau_{\text{max}}x^a$ ,  $\tau_{\text{max}} = 20$ ,  $a = 4$

Gaussian:  $\tau(x) = \tau_{\text{max}}e^{-[(x-1)/b]^2}$ ,  $\tau_{\text{max}} = 18$ ,  $b = 0.4$

Step function:  $0 < x < x_0$   $\tau(x) = 0$ ,  $x_0 < x < 1$   $\tau(x) = \tau_{\text{max}}$ ;  $\tau_{\text{max}} = 5$ ,  $x_0 = 0.3$

Two dashed lines bracket the interval  $0.5 < \tau < 3$ . As can be judged from the inset table, the residual intensity ( $I$ ) is mainly decided by the extent of the  $\tau < 0.5$  absorber ( $T$ ). For any distribution, material with  $\tau > 3$  has negligible effect on the trough since less than 5% ( $e^{-3}$ ) of the flux at any given point is being transmitted.

### 3. FORMATION OF DOUBLET TROUGHS

Depending on which model we use for the absorber, the residual intensity in a single absorption trough can yield vastly different estimates for the optical depth that causes it. We know that the apparent optical depth method, which works so well for the ISM and IGM absorbers, is a very poor model for many AGN outflows troughs, where  $\tau_{ap} \equiv -\log(I)$  gives only a lower limit for the real optical depth. This is evident when more troughs from the same ion are added as constraints on our absorbing model. Several doublet lines commonly produce absorption troughs in the spectrum of AGN outflows, the most notable are C IV  $\lambda\lambda 1548.20, 1550.77$ , N V  $\lambda\lambda 1238.82, 1242.80$  and O VI  $\lambda\lambda 1031.93, 1037.62$ . These lines provide sufficient constraints to test the apparent optical depth method. For all the above doublets, the oscillator strength of the blue (the shorter wavelength) transition is exactly twice that of the red transition. Therefore, the expected optical depth ratio is almost exactly 2:1 in favor of the blue transition. (It is not exactly 2:1 since the wavelengths differ by a small amount.) For the apparent optical depth method to hold, we must have  $\tau_{ap}(\text{blue}) = 2\tau_{ap}(\text{red})$  which requires:  $I_B = I_R^2$ , where  $I_B$  and  $I_R$  are the residual intensities of the blue and red absorption troughs, respectively. For ISM and IGM absorber this relationship holds to an excellent degree (Arav et al. 2001a). In contrast, in most AGN outflow troughs we find  $I_B \neq I_R^2$ , instead we detect the whole range  $I_R \geq I_B \geq I_R^2$ . (Values outside this range are unphysical and usually can be attributed to the errors associated with the data [Hamann et al. 1997].)

In order to explain the observed  $I_R \geq I_B \geq I_R^2$ , the standard method is to invoke partial covering of the emission source. In its simplified form, we assume that the absorber covers only a portion  $C$  (which generally depends on the velocity) of a constant emission source (at a given  $\lambda$ ). We further assume that the  $\tau$  distribution in front of the covered part of the source is constant. With these assumptions, the absorption equations are:

$$I_R(v) - (1 - C(v)) = C(v)e^{-\tau(v)} \quad (2)$$

$$I_B(v) - (1 - C(v)) = C(v)e^{-2\tau(v)}, \quad (3)$$

where  $v$  is the velocity of the outflow,  $C(v)$  is the effective covering fraction (see Arav et al. 1999b), and  $\tau(v)$  is the optical depth of the red doublet component. From these two equations we obtain:

$$C(v) = \frac{I_R(v)^2 - 2I_R(v) + 1}{I_B(v) - 2I_R(v) + 1}, \quad \tau(v) = -\ln\left(\frac{I_R(v) - I_B(v)}{1 - I_R(v)}\right), \quad (4)$$

By construction, the partial covering model will always give a  $C(v)$  and  $\tau(v)$  solution to equations (2) and (3), provided that  $I_R \geq I_B \geq I_R^2$ . In order to test the validity of the model we must work with more than two lines from the same ion (see Gabel et al. 2004).

For the inhomogeneous absorber we need to test if, and under what conditions, the absorber satisfies the constraints imposed by doublet lines. In doing so we make use

of and expand the simulation results derived by dKKA, followed in the next section by applying these results to data of Mrk 279. To simulate doublet data, we start by computing the residual intensity for a given power-law distribution  $\tau(x) = \tau_{\max}x^a$ , thus obtaining  $I(\tau_{\max}, a)$ . We define the red doublet residual intensity to be  $I_R \equiv I(\tau_{\max}, a)$  and obtain the blue doublet residual intensity, by using twice the  $\tau_{\max}$  value for the same distribution,  $I_B = I(2\tau_{\max}, a)$ . To obtain a meaningful comparison between different power-law ( $a$ ) distributions we convert the resulting  $I(\tau_{\max}, a)$  to  $I(\bar{\tau}, a)$ . Apart from the last step, this is the same procedure dKKA used for producing their figure (2). However, unlike dKKA, we begin with looking at a single velocity position. This is done in order to gain better understanding for the formation of doublet troughs from inhomogeneous absorbers. We discuss the velocity dependency in the next section. Following the power-law simulation we repeated the same procedure to produce doublet simulations from gaussian distributions.

Figure 2 shows the simulated results for two power law distributions,  $a = 1$  and  $a = 8$ . The simulated  $I_R$  and  $I_B$  are displayed as well as  $I_R^2$ . As discussed above, for a given  $I_R$  the allowed physical range of  $I_B$  is always between  $I_R$  and  $I_R^2$ , and it is important to keep in mind the narrowness of the physically allowed range when comparing power law fits to actual doublet data. Also shown is  $1 - C$  where  $C$  is the covering factor one would derive using the pure partial covering equations (4) for the simulated  $I_R$  and  $I_B$ . A common result from analyzing real data is that the  $1 - C$  curve is almost identical with  $I_B$ . In the simulations, we observe that for large enough  $\bar{\tau}$  (roughly above 3 in both cases),  $1 - C$  is indeed almost identical with  $I_B$ . As was found by dKKA, we confirm that for a shallow power-law ( $a = 1$ ),  $1 - C$  is consistent with  $I_B$  only for  $0 < I_B < 0.1$ , and for a steep power-law ( $a = 8$ )  $1 - C$  is consistent with  $I_B$  for  $0 < I_B < 0.6$ . However, in the steep power-law case, it is difficult to obtain low values of  $I_B$ . In the example shown,  $I_B = 0.35$  only at  $\bar{\tau} = 300$ . The dashed curves show the ratio of  $\bar{\tau}/\tau_{\text{doublet}}$  (read from the right axis), where  $\tau_{\text{doublet}}$  is the optical depth derived by using the pure partial covering equations (4). This ratio is a good indicator for the amount of “hidden” column density in the inhomogeneous absorber compared to what we deduce from the pure partial covering model. We note that  $\tau_{\text{doublet}} \geq \tau_{\text{ap}}$ , therefore  $\bar{\tau}/\tau_{\text{ap}}$  will be correspondingly larger.

Let us look at the mechanism which creates the simulated  $I_R$  and  $I_B$  for the steep power-law ( $a = 8$ ). This case is interesting since for a given  $\tau$ ,  $I_R$  and  $I_B$  are quite close in value and  $I_R - I_B$  is considerably smaller than  $I_R - I_R^2$  or  $I_B - I_R^2$ . Such a situation is often seen in real outflow data. The driver behind the finite yet small  $I_R - I_B$  is closely related to the area of the absorber that is covered by small optical depth. For this purpose we defined the transmission parameter  $T$ , which measures the fraction of the emission source that is covered by  $\tau < 0.5$ . We find that for steep power-laws,  $T$  is almost identical with the residual intensity. For example, for  $\bar{\tau} = 50, I = 0.41, T = 0.40$  and for  $\bar{\tau} = 100, I = 0.37, T = 0.36$ . Since the ratio of  $\bar{\tau}$  in these two examples is 2, the residual intensities can be taken as  $I_B(\bar{\tau} = 100)$  and  $I_R(\bar{\tau} = 50)$  (which is how figure 2 was made).  $I_R - I_B$  is almost fully attributed to  $\Delta T$ , which suggests a simple geometrical interpretation:



The residual intensities are mainly determined by the optically thin ( $0.5 > \tau$ ) extent of the absorber over the emission source ( $T$ ), and the difference in doublet intensities,  $I_R - I_B$ , is almost entirely explained by the  $\Delta T$  of the two distributions.

Figure 3 shows the simulated results for two gaussian distributions,  $b = 0.4$  and  $b = 0.2$ . The additional dashed curves give  $T_R$  and  $T_B$  the transmission parameter for the red and blue troughs respectively. It is evident that  $I_R \simeq T_R$  and  $I_B \simeq T_B$  (as is the case for steep power-law distributions). Even for broader gaussians ( $b = 0.4$ ) this approximation is good to within 10% – 20% across most of the  $\bar{\tau}$  range. Comparing figures 2 and 3 we see that there is little qualitative difference between the troughs produced by power-laws and gaussians. This is expected since the behavior of both functions in the  $\tau < 3$  region is quite similar for steep and high  $\tau_{\max}$  cases (see Fig. 1). Since the results of power-law and gaussian models are very similar, we will concentrate on power-laws in the rest of this paper.

Having  $I_R - I_B$  small but finite at high  $\bar{\tau}$  is both a strength and a weakness for the inhomogeneous absorber model. In real high-quality data, we often see occurrences that look like the lower panel of figure 2. That is,  $I_B$  is close to, but distinctively smaller than  $I_R$  while  $I_B$  is considerably larger than  $I_R^2$  (the homogeneous full coverage absorber model). These occurrences are statistically difficult to explain using the pure partial coverage model (eqs. 2 and 3), where for  $\tau_{red} > 3$ ,  $I_R - I_B \simeq 0$ . We are therefore left with the question of why in so many outflow absorbers, mother nature chose optical depth  $0.5 < \tau_{red} < 3$  (Below  $\tau_{red} = 0.5$  it is difficult to distinguish between the homogeneous full coverage absorber and the pure partial coverage models.). As shown in figure 2, inhomogeneous absorber models can produce a small but finite  $I_R - I_B$  at much higher  $\bar{\tau}$  values. The weakness is related to the observed examples of  $I_R - I_B \simeq 0$ , which of course reverses the argument.  $I_R - I_B \simeq 0$  is naturally explained as  $\tau_{red} > 3$  occurrences for the pure partial coverage model. However, the inhomogeneous power-law absorber models maintain a finite  $I_R - I_B$  even at absurdly high values of  $\bar{\tau}$ . This point is strengthened by the fitting of O VI doublet troughs in the Mrk 279 data (§ 5.2). A related weakness of inhomogeneous power-law absorber models is their inability to create small values of  $I_R, I_B$  for steep distributions (e.g., the  $a = 8$  example in fig. 2) and reasonable values of  $\bar{\tau}$ . Shallow power-law distributions can do so but at the cost of having unrealistically large  $I_R - I_B$  values. In the following section we will test these conjectures on real outflow data.

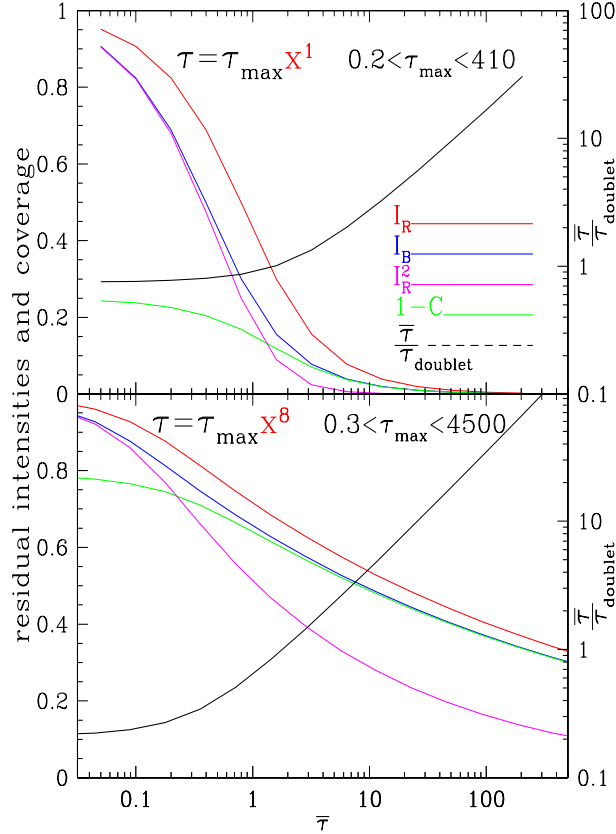


Fig. 2.— Formation of doublet troughs from power-law distributions of absorbing material (given at the top of each panel). For both distributions we display the following results: red, residual intensity of the red doublet component ( $I_R$ ); blue, residual intensity of the blue doublet component ( $I_B$ ), which is created by doubling the optical depth used to simulate  $I_R$ ; magenta,  $I_R^2$ , what  $I_B$  would have been for complete coverage homogeneous absorber; green,  $1 - C$  where  $C$  is the covering factor one would derive using the pure partial covering equations (4) for the simulated  $I_R$  and  $I_B$ ; black  $\bar{\tau}/\tau_{\text{doublet}}$  (read from the right axis), where  $\tau_{\text{doublet}}$  is the optical depth derived by using the pure partial covering equations (4).

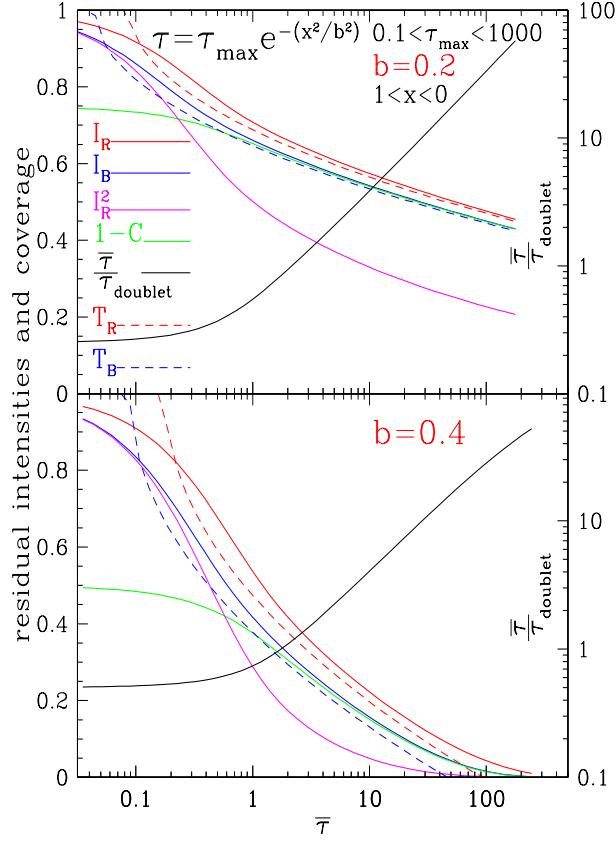


Fig. 3.— Formation of doublet troughs from gaussian distributions of absorbing material (see top panel). The presentation is similar to that of Fig. 2 with two additional dashed curves, which show the transmission parameter for the gaussian distributions:  $T_R$  and  $T_B$  are for the distribution that produces  $I_R$  and  $I_B$ , respectively. For the narrow  $b = 0.2$  gaussian it is evident that  $I_R \simeq T_R$  and  $I_B \simeq T_B$  (as is the case for steep power-law distributions). Even for broader gaussians ( $b = 0.4$ ) this approximation is good to within 10% – 20% across most of the  $\bar{\tau}$  range.

## 4. FITTING REAL DATA

On May 2003 we obtained simultaneous X-ray and UV observations of the Mrk 279 AGN outflow. (Description of the UV observations is found in Gabel et al. 2004, and the X-ray observations in Costantini et al. 2004.) The 92 ksec FUSE data yielded the highest quality O VI trough-spectrum of any AGN outflow to date, and the 16 orbits HST/STIS/E140M observation yielded high quality N V troughs. The combined HST/FUSE spectrum gives high signal-to-noise Ly $\alpha$ , Ly $\beta$  and Ly $\gamma$  troughs. In this section we use the inhomogeneous absorber formalism developed in the previous section to fit these data and check whether these simple distributions are an adequate model for real outflow troughs.

To fit the O VI and N V troughs with inhomogeneous absorber models we start by normalizing the data, which is done by dividing the observed flux by an unabsorbed emission model. In doing so we implicitly assume that the inhomogeneous absorber has the same characteristics in front of both the continuum and BEL sources. We then fit the red doublet data at each velocity bin as follows: we choose a power law value and using the formalism described in § 2 iterate until a specific  $\tau_{\max}$  gives us the observed value of  $I_R$ . We use the  $\bar{\tau}$  of this distribution when comparing with the optical depth  $\tau_{\text{doublet}}$  derived from the doublet equations (4). Following the procedure described in § 3, we double the fitted  $\tau_{\max}$  and take the residual intensity from the same distribution with  $2\tau_{\max}$  as  $I_B$ . This process is repeated for all the velocity bins in the trough. If the simulated  $I_B$  curve for any given power-law index gives a good fit for the entire observed  $I_B$  trough, we will have a strong indication that the material is indeed inhomogeneously distributed, with a specific power law. A similar fitting procedure is used for the Lyman series troughs.

### 4.1. O VI Troughs

In figure 4 we show the O VI fitting results for two power-law models. It is clear that the  $a = 1$  case gives a poor fit to the blue doublet-component data for most of the velocity range  $-500 < v < -230$  km s $^{-1}$ . This is mainly due to the inability of a shallow power law to produce  $I_B \sim I_R$  (see Fig. 2). A steeper power-law ( $a = 4$ ) does a much better job in fitting the  $I_B \sim I_R$  parts of the trough, but cannot reproduce the regions where  $I_B$  is roughly half way between  $I_R$  and  $I_R^2$ . The general behavior is shown in the lower panel of figure 5, where we re-normalize the O VI data by dividing all the curves by  $I_R$ . In this presentation  $I_R = 1$  and the behavior of  $I_B$  with respect to  $I_R$  is made clearer. Moreover, we can now examine four power-law models and better quantify their relationship to  $I_B$  and  $I_R$ . We observe that the ratio  $I_B/I_R$  is not constant and shows considerable structure. In contrast, for steep power-laws that give better overall fits to  $I_B$ , the ratio of simulated  $I_B/I_R$  is constant. These contrasting behaviors explain why steep power-law (or narrow gaussian) models do not provide a good fit for the entire  $I_B$  trough.

However, the main problem with steep power-law (or narrow gaussian) models is the unrealistic high value of  $\bar{\tau}$  necessary to obtain the observed  $I_R$ . This issue was already discussed in the simulation of doublet data (§ 3). In the upper panel of figure 5 we show the  $\bar{\tau}$  curves for the models shown in figure 4 and the lower panel of 5. The steep power-law models ( $a = 2, 4$ ), which provide a better fit for most of the observed trough, necessitate high  $\bar{\tau}$ . This behavior is an artifact of the need to have a steep power-law model with a small  $T$  parameter. We conclude that simple power-law and gaussian distributions are hard pressed to fit the Mrk 279 high-quality O VI trough data.

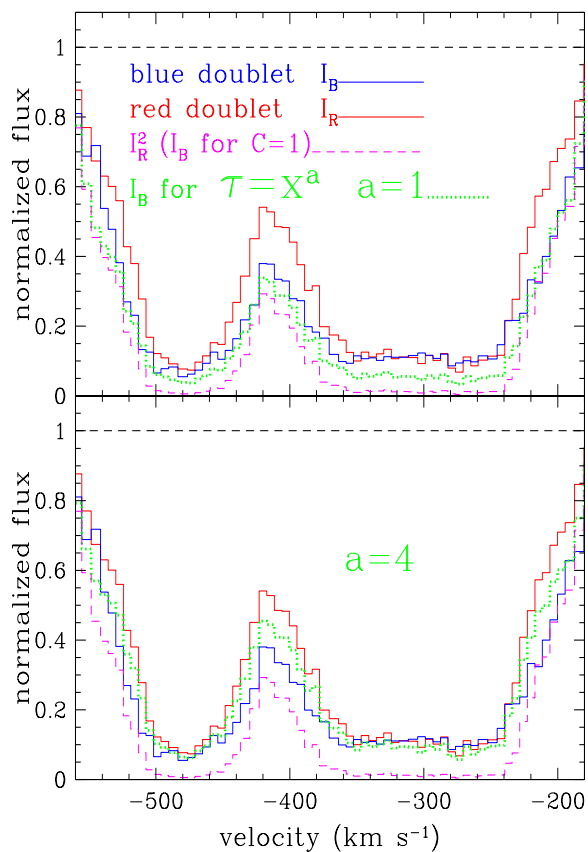


Fig. 4.— Power-law fits to the O VI outflow troughs seen in Mrk 279 (2003, FUSE spectrum). The normalized data for the red and blue doublet troughs are plotted, as well as  $I_R^2$ , which is the expected value of  $I_B$  for complete coverage homogeneous absorber. The physically allowed range of  $I_B$  for any material distribution is between the  $I_R$  and  $I_R^2$  curves. For the chosen power-law model we show the predicted  $I_B$  from the same distribution that gave an exact match to the observed  $I_R$ .

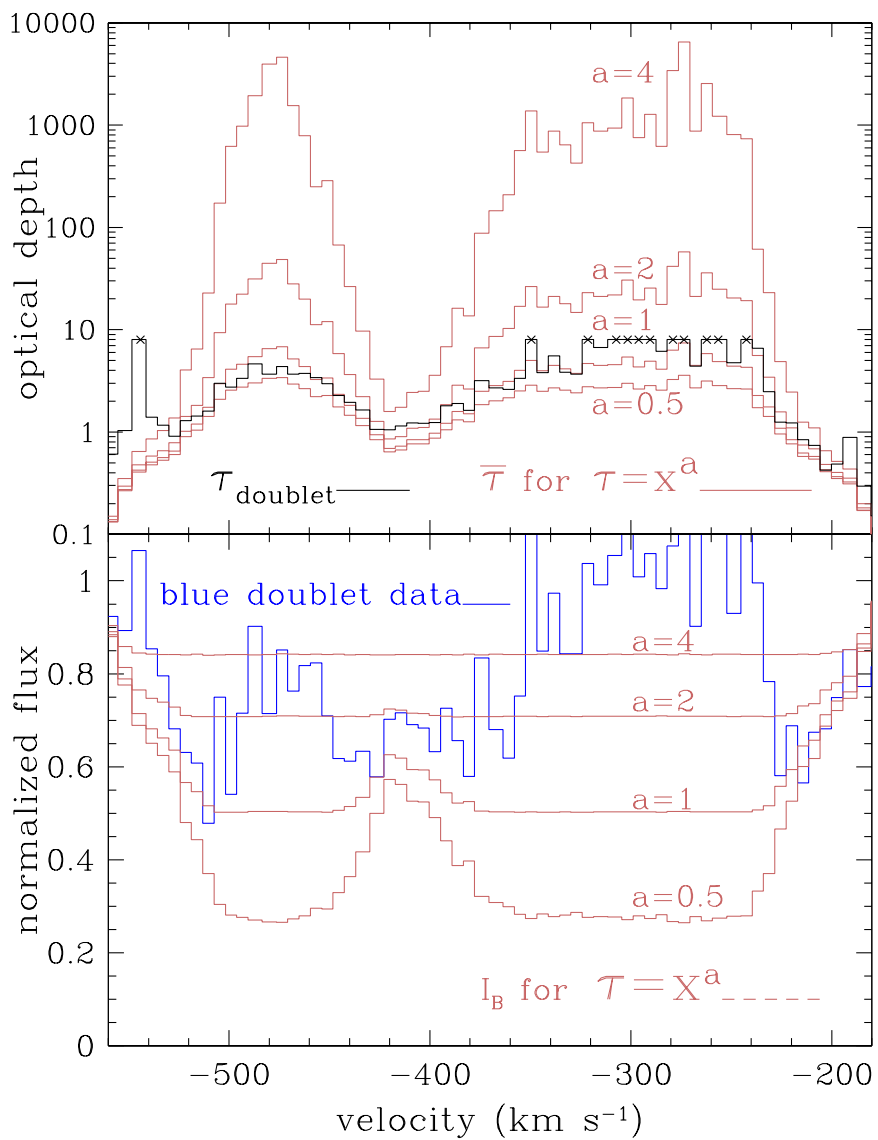


Fig. 5.— Four power-law fits for the Mrk 279 O VI outflow troughs. The data shown in Fig. 4 were renormalized by dividing all the curves by  $I_R$ . This allows us to compare several solutions and examine the behavior of  $I_B/I_R$ . In this presentation, it is clear that none of the  $I_B$  solutions fits the blue doublet well. A combination of power-laws with  $1 < a < 10$  is needed to fit the full blue trough.

## 4.2. N v Troughs

The situation is quite different for the N v troughs. Figure 6 shows the fitting results for an  $a = 1$  power-law model that fit the data quite well. Examining figure 7 shows that power-law models with  $1 < a < 2$  yield good fits except at  $v > -260 \text{ km s}^{-1}$ . Moreover, the inferred optical depth values are generally in good agreement with the doublet solution. The two exceptions are the expected departure at  $v > -260 \text{ km s}^{-1}$  and at  $-400 > v > -450$ , where the doublet solution is suspect due to the shallowness of the absorption data.

We conclude that by themselves, the N v troughs give support to simple inhomogeneous absorber models (even for a model with a constant gradient). A reasonable fit is produced with only one velocity-dependent free parameter (the optical depth), compared to the partial covering model that requires two free parameters at each velocity point (optical depth and covering fraction). However, as we elaborate in the discussion, much of this result can be attributed to the lower real optical depth on the N v troughs combined with the mathematical attributes of the power-law fits.



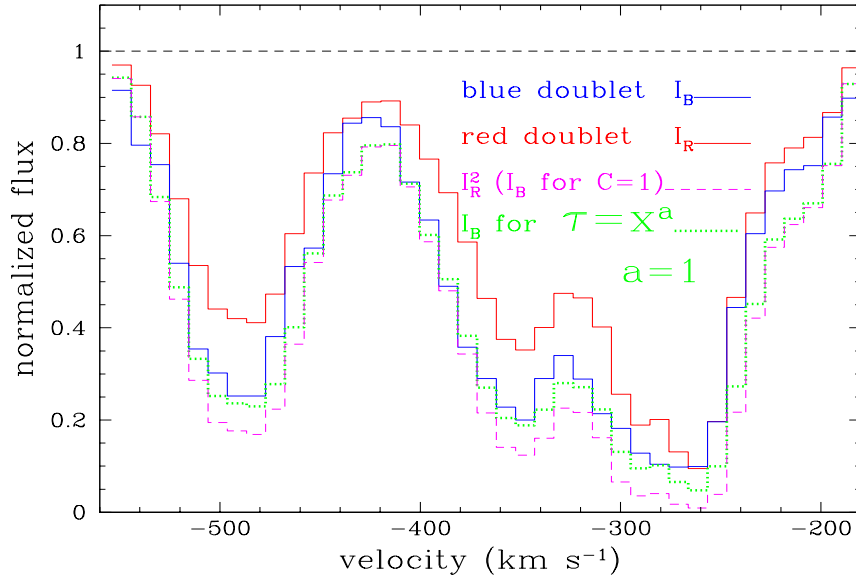


Fig. 6.— Power-law fit to the NV outflow troughs seen in Mrk 279 (2003, HST/STIS spectrum), same presentation as Fig. 4.

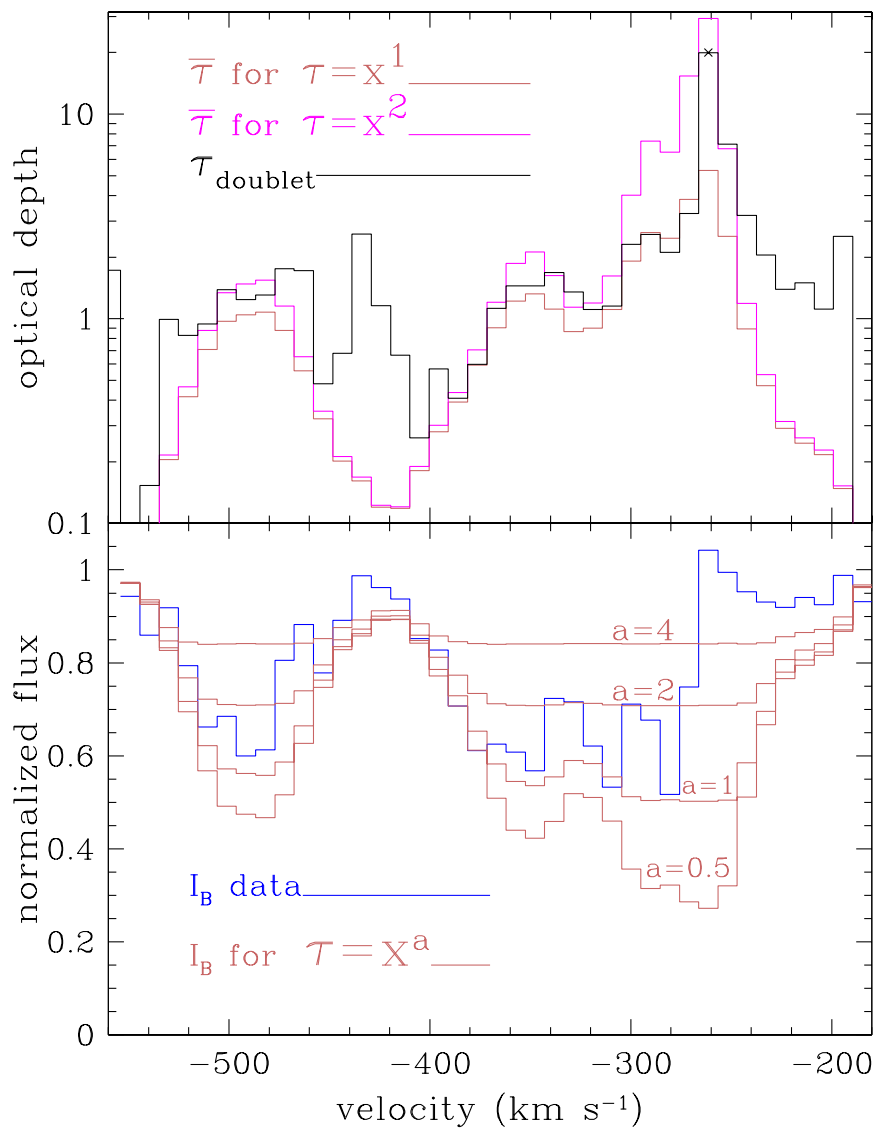


Fig. 7.— Optical depth ( $\bar{\tau}$ ) for the four solutions shown in Fig. 5 and the  $\tau_{\text{doublet}}$  solution for comparison. The crosses at the highest  $\tau_{\text{doublet}}$  values donate lower limits. It is clear that the better fit power-law models ( $a=2$  and 4) require an enormous  $\bar{\tau}$  for obtaining the fit, while those with more acceptable  $\bar{\tau}$  ( $a = 0.5$  and 4) do not yield a good fit for  $I_B$  (see Figs. 4 and 5).

### 4.3. Lyman Series Troughs

A more stringent test for simple inhomogeneous absorber models is available by fitting the Lyman series troughs. In the combined HST/FUSE spectrum of Mrk 279 we have high-quality data for moderately deep troughs from Ly $\alpha$ , Ly $\beta$  and Ly $\gamma$ . Fitting three troughs from the same ion is far more constraining than fitting a doublet. For a doublet, we use one of the troughs as a baseline, that is, we construct the model to give it a perfect fit. The same model is then used to fit the other doublet component as described in § 4.1. A degree of freedom (in our case the power-law exponent) may very well suffice to fit the single remaining trough. For the three Lyman series troughs, we fit Ly $\beta$  in the same way we fitted the red doublet component of O VI and N V, but now the same model has to fit both Ly $\alpha$  and Ly $\gamma$ . To fit the Ly $\alpha$  trough we take the derived  $\tau_{\max}(\text{Ly}\beta)$  and multiply it by the expected ratio of optical depths between Ly $\alpha$  and Ly $\beta$ :  $\tau_{\text{Ly}\alpha}/\tau_{\text{Ly}\beta} = (\lambda_{\text{Ly}\alpha}f_{\text{Ly}\alpha})/(\lambda_{\text{Ly}\beta}f_{\text{Ly}\beta})$ , where  $\lambda$  and  $f$  are the wavelength and oscillator strength for each transition. We then use this value as  $\tau_{\max}(\text{Ly}\alpha)$  for the same power law model in order to arrive at the expected Ly $\alpha$  residual intensity. The procedure to fit Ly $\gamma$  is similar.

As described in Scott et al. (2004) and Gabel et al. (2004) the Lyman series troughs are partially contaminated by non-outflow related absorption. Only the absorption in the velocity range  $-350 < v < -200$  is considered to be purely outflow related in the Lyman series troughs, and therefore we only fit this region. The high ionization CNO doublets are not affected by this unrelated absorption, which allows us to fit their entire profile. In figure 8 we show the fitting results for three power-law models. While the  $a = 1$  model gives a reasonable fit for the Ly $\gamma$  data, it strongly over predicts the depth of the Ly $\alpha$  trough. A Steeper power law  $a = 4$  gives an adequate fit to the Ly $\alpha$  trough, but greatly over predicts the depth of the Ly $\gamma$  trough. A middle model ( $a = 2$ ) gives unsatisfactory fits for both Ly $\alpha$  and Ly $\gamma$ . It is clear that simple power-law inhomogeneous absorber models are not an adequate model for the Lyman series outflow troughs in Mrk 279.

## 5. DISCUSSION

In § 4 we attempted to fit the outflow troughs of Mrk 279 with simple power-law inhomogeneous absorber models. We demonstrated that the O VI troughs cannot be fitted well with such models. The main reason for that was the small differences between  $I_B$  and  $I_R$  across most of the velocity profile. The extreme occurrence is in the velocity range  $-360 < v < -240$  where  $I_B$  and  $I_R$  are indistinguishable within the noise limits. This part of the trough can only be fitted by inhomogeneous models that will closely resemble the step-function shown in figure 1. Therefore, the velocity range  $-360 < v < -240$  of the O VI troughs strongly supports the physical picture of the partial covering model and advocates for an optical depth distribution with a sharp edge.

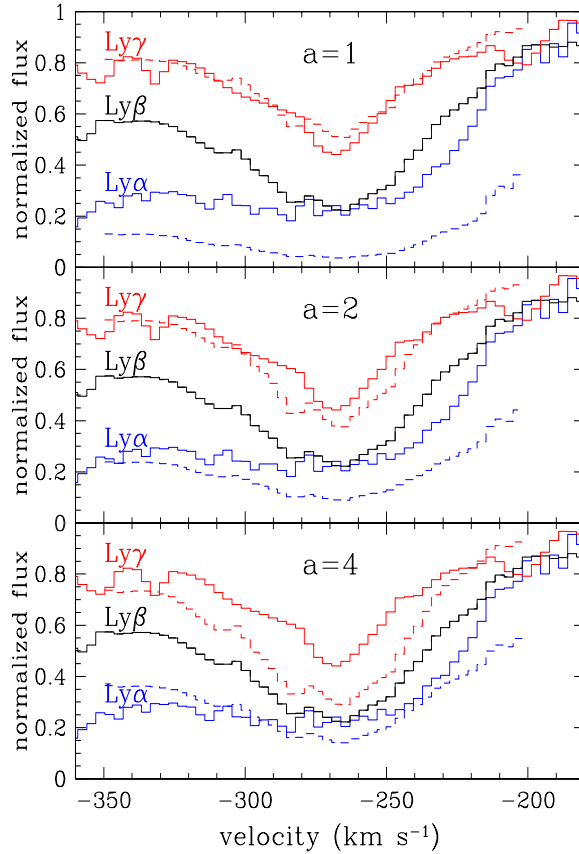


Fig. 8.— Power-law fits to the Lyman series outflow troughs seen in Mrk 279 (2003, FUSE and HST spectrum). The normalized data are plotted as solid histograms. Errors in the normalized data are dominated by systematic effects (mainly in the level of the unabsorbed emission model), which are smaller than 5% for each curve (Gabel et al. 2004). Each panel shows a power-law model ( $\tau = x^a$ ) fit for Ly $\alpha$  and Ly $\gamma$  (dashed histograms, color matched to the data). By construction the models give a perfect fit to Ly $\beta$ . From the range of plotted models, it is clear that no power-law model can simultaneously fit Ly $\alpha$  and Ly $\gamma$ .

In contrast the N v troughs were well-fitted by a simple inhomogeneous power-law absorber model. By itself this is quite a remarkable fit since we only let the optical depth vary as a function of velocity, where the partial covering model requires both the optical depth and the covering fraction to be velocity dependent free parameters. Such a situation was found by dKKA for the Si IV troughs in BALQSO 1603+3002. However, for the Mrk 279 data similar models could not reasonably fit the O VI troughs nor the Lyman series troughs. We should therefore look at the mathematical behavior of the power-law fits and see whether it can explain the goodness of the N v fit irrespectively of the actual physical model. We can attribute the success of the N v fit to the fact that for these troughs  $I_B$  is roughly in between  $I_R$  and  $I_R^2$ . As shown in figure 2, such occurrence with similar residual intensities can be reproduced by a shallow power-law model (e.g.,  $a = 1$ ) that produces almost identical  $\bar{\tau}$  and  $\tau_{\text{doublet}}$ . It is plausible that the good N v fit is simply a result of the moderate optical depth for this ion.

As discussed in § 4.3, the strongest constraints on simple inhomogeneous absorber models come from the attempt to fit the Lyman series troughs. In this case it is evident that even allowing for complete freedom of both the power-law exponent and the optical depth as a function of velocity will not yield an acceptable fit. In contrast, partial covering models do yield good fits for the Lyman series troughs (Gabel et al. 2004). The success of partial covering models, combined with the failure of the inhomogeneous absorber models, suggest a sharp edge in the optical depth distribution across the source. We note that calculations of synthetic line profiles, based on wind models with the extended continuum source, support our notion of the optical depth distribution with a sharp edge (e.g., Proga 2003, and references therein). Partial covering models are equivalent to a step function distribution of optical depth across the absorber. Mathematically, step functions, gaussians and a power-law distributions all have two free parameters. Therefore, the comparison between the models stands on firm grounds. We conclude that monotonic inhomogeneous absorber models that do not include a sharp edge in the optical depth distribution across the source are not an adequate physical model to explain the trough formation mechanism for the outflow observed in Mrk 279.

## ACKNOWLEDGMENTS

This work is based on observations obtained with *HST* and *FUSE*, both built and operated by NASA. Support for this work was provided by NASA through grants number *HST*-AR-9536, *HST*-GO-9688, *HST*-GO-9688, from the Space Telescope Science Institute, which is operated by the Association of Universities for Research in Astronomy, Inc., under NASA contract NAS5-26555, and through *Chandra* grant 04700532 and by NASA LTSA grant 2001-029. The National Laboratory for Space Research at Utrecht is supported financially by NWO, the Netherlands Organization for Scientific Research. We also thank Yuri Levin for a thorough reading of the manuscript.

## REFERENCES

- Arav, N., 1997 in Mass Ejection from AGN, ASP Conference Series, Vol. 128, ed. N. Arav, I. Shlosman, and R. J. Weymann, p. 208
- Arav, N., Korista, T. K., de Kool, M., Junkkarinen, V. T. & Begelman, M. C. 1999, ApJ, 516, 27. (1999a)
- Arav, N., Becker, R. H., Laurent-Muehleisen, S. A., Gregg, M. D., White, R. L., Brotherton, M. S., & de Kool, M. 1999, ApJ, 524, 566 (1999b)
- Arav, N., Brotherton, M. S., Becker, R. H., Gregg, M. D., White, R. L., Price, T., Hack, W. 2001, ApJ, 546, 140 (2001a)
- Arav, N., et al. 2001, ApJ, 561, 118 (2001b)
- Arav, N., Korista, T. K., de Kool, M., 2002, ApJ, 566, 699
- Arav, N., et al. 2004, in preperation
- Barlow, T. A., 1997 in Mass Ejection from AGN, ASP Conference Series, Vol. 128, ed. N. Arav, I. Shlosman, and R. J. Weymann, p. 13
- Costantini, E., et al. 2004, in preperation
- Churchill, C. W., Schneider, D. P., Schmidt, M., Gunn, J. E., 1999, AJ, 117, 2573
- Crenshaw, D. M., Kraemer, S. B., Boggess, A., Maran, S. P., Mushotzky, R. F., Wu, C. C., 1999 ApJ, 516, 750
- de Kool, M., Arav, N., Becker, R. H., Laurent-Muehleisen, S. A., White, R. L., Price, T., Gregg, M. D. 2001, ApJ, 548, 609
- de Kool, M., Korista, K. T., Arav, N., 2002, ApJ, 580, 54
- Gabel, J. R., et al. 2003, ApJ, 583, 178
- Gabel, J. R., et al. 2004, in preperation
- Ganguly, R., Eracleous, M. C., Charlton, J. C., & Churchill, C. W. 1999, AJ, 117, 2594

- Hamann, F., Barlow, T. A., Junkkarinen, V., Burbidge, E. M., 1997, *ApJ*, 478, 80
- Kaastra, J. S., Mewe, R., Liedahl, D. A., Komossa, S., Brinkman, A. C., 2000, *A&A*, 354L, 83
- Kaastra, J. S., Steenbrugge, K. C., Raassen, A. J., van der Meer, R., Brinkman, A. C., Liedahl, D. A., Behar, E., de Rosa, A., 2002, *A&A*, 386, 427
- Kaspi, S., Brandt, W. N., Netzer, H., Sambruna, R., Chartas, G., Garmire, G. P., Nousek, J. A., 2000, *ApJ*, 535L, 17
- Kaspi, S., & Netzer, H. 1999, *ApJ*, 524, 71
- Kriss, G. A., Green, R. F., Brotherton, M., Oegerle, W., Sembach, K. R., Davidsen, A. F., Friedman, S. D., Kaiser, M. E., Zheng, W., Woodgate, B., Hutchings, J., Shull, J. M., York, D. G., 2000, *ApJL*, 538, 17
- Korista, T. K., Voit, G. M., Morris, S. L., & Weymann, R. J. 1993, *ApJS*, 88, 357
- Proga, D., 2003, *ApJ*, 592, 9
- Scott, J. E., 2004, *ApJS*, 152, 1
- Telfer, R.C., Kriss, G.A., Zheng, W., Davidson, A.F., & Green, R.F. 1998, *ApJ*, 509, 132
- Weymann, R. J., Morris, S. L., Foltz, C. B., & Hewett, P. C. 1991, *ApJ*, 373, 23